GAUSSIAN MIXTURE MODEL FOR HYPERSPECTRAL UNMIXING WITH LOW-RANK REPRESENTATION

Qiwen Jin[1], *Yong Ma*[1,2], *Xiaoguang Mei*[1,2,*], *Xiaobing Dai*[1,2], *Hao Li*[3], *Fan Fan*[1,2], *Jun Huang*[1,2]

[1]Electronic Information School, Wuhan University, Wuhan, 430072, China
[2]Institute of Aerospace Science and Technology, Wuhan university, Wuhan, 430072, China
[3]School of Mathematics and Computer Science, Wuhan Polytechnic University, Wuhan 430023, China

ABSTRACT

Gaussian mixture model (GMM) can estimate not only the abundances and distribution parameters but also distinct endmember set for each pixel. However, the traditional GMM unmixing model only has proper smoothness and sparsity prior constraints on the abundances and thus cannot excavate the local spatial information in hyperspectral image (HSI). Thus, we propose a new unmixing method with superpixel segmentation (SS) and low-rank representation (LRR) based on GMM called GMM-SS-LRR, which can consider the local spatial correlation of HSI. First, we adopt the principal component analysis (PCA) to obtain the first principal component of HSI, which contains the most information for the entire HSI. Then, we adopt the SS in the first principal component of HSI to obtain the homogeneous regions, and the abundances in each homogeneous region have the underlying low-rank property. Finally, we unmix the pixels in each homogeneous region of HSI depending on the low-rank property of abundances. Experiments on synthetic datasets and real HSIs demonstrate that the proposed GMM-SS-LRR is efficient compared with other current popular methods.

Index Terms— Hyperspectral image analysis, Gaussian mixture model, superpixel segmentation, low-rank property

1. INTRODUCTION

Hyperspectral image (HSI) has rapidly developed into a powerful technology in the field of earth observation and geoinformation science. The wealth of spatial and spectral information has facilitated the use of HSI in many applications, such as spectral unmixing, object classification, and matching [1, 2, 3, 4, 5]. However, accurate interpretation of HSI is difficult due to the low spatial resolution together with the mixing effects of the ground surfaces and given that a single pixel is made up of several different materials. Therefore, spectral unmixing is an essential step for the deep exploitation of HSI.

The formation of HSI can be simplified by the *linear mixing model* (LMM), which assumes that the physical region corresponding to a pixel contains several pure materials. LMM has been widely used due to its simplicity and physical meaning. Bayesian framework methods have also been receiving considerable attention in HSI unmixing, with which not only can we incorporate prior distribution but also estimate hyperparameters conveniently. Numerical methods based on Bayesian have been proposed. In [6], Eches *et al.* proposed the normal compositional model (NCM), which assumes the endmembers for each pixel are sampled from unimodal Gaussian distribution; then, NCM uses different optimization approaches, such as expectation maximization [7], sampling method [8], and particle swarm optimization [9], to determine the hyperparameters. In [10], Du *et al.* proposed a Beta compositional model (BCM) to model the endmember variability in the HSI unmixing. Zhou *et al.* proposed the Gaussian mixture models (GMMs) with proper smoothness and sparsity prior constraints on the abundances [11]. However, these unmixing methods ignore the spatial correlation of HSI despite the importance of spatial information in the application of HSI. In HSI, the correlations of the adjoining bands and the adjacent pixels are usually high, which introduces the underlying low-rank property to the original HSI in the local patch. Qu *et al.* proved that the abundance matrix has low-rank property in homogeneous region and constructed an unmixing model by using low-rank property to verify the effectiveness in homogeneous region unmixing [12].

Thus, in this paper, we propose a novel GMM based on superpixel segmentation (SS) and low-rank representation (LRR), which is called GMM-SS-LRR, to solve the above problems. We adopt the adaptive size superpixel strategy to customize the shape and size of the unmixing region on the basis of different spatial structures and consider each superpixel as a non-overlapping region. The super segmentation in the original will introduce low-rank property to the pixels in each homogeneous region, thereby fully utilizing the spatial correlation in HSI. With low-rank constraints on the abundances, the conditional density function leads to a standard maximum a posteriori (MAP) problem, which can be solved using generalized expectation maximization (GEM) [13].

*Corresponding author (email: meixiaoguang@gmail.com).

This research was funded by the National Natural Science Foundation of China under grant nos. 61805181, 61705170, 61773295 and 61605146.

2. METHODOLOGY

2.1. Gaussian mixture model (GMM) framework

GMM method [11] is an LMM. GMM takes the following route to formulate the HSI for modeling real scenarios accurately:

$$\mathrm{y}_n = \sum_{j=1}^{M} \mathrm{m}_{nj}\alpha_{nj} + \mathrm{n}_n, \tag{1}$$

where $\mathrm{y}_n \in \mathbb{R}^B$ is the observed spectra (B is the number of wavelengths and N is the number of pixels), $\mathrm{m}_{nj} \in \mathbb{R}^B$: $j = 1, \ldots, M$ is the pure material spectra (called *endmember*), and M is the number of endmembers, α_{nj} is the proportion (called *abundance*) for the jth endmember at the nth pixel (with the positivity and sum-to-one constraint), and n_n is the additive noise. Here, m_{nj} indicates that the endmember spectra for each pixel can be different. This condition is called *endmember variability*.

GMM method assumes that m_{nj} follows the GMM, and noise n_n follows the Gaussian distribution: $p(\mathrm{n}_n) := \mathcal{N}(\mathrm{n}_n|0, \mathrm{D})$, where D is the noise covariance matrix. Using Eq. (1), we can obtain the density function of y_n as follows:

$$p(\mathrm{y}_n|\boldsymbol{\alpha}_n, \boldsymbol{\Theta}, \mathrm{D}) = \sum_{\mathrm{k}\in\mathcal{K}} \pi_\mathrm{k}\mathcal{N}\left(\mathrm{y}_n|\boldsymbol{\mu}_{n\mathrm{k}}, \boldsymbol{\Sigma}_{n\mathrm{k}}\right) \tag{2}$$

where $\mathcal{K} := \{1, ...K_1\} \times \{1, ...K_2\} \times ... \times \{1, ...K_M\}$ is *the Cartesian product of the M index sets*, k:=$(k_1, ...k_M) \in \mathcal{K}$, $\pi_\mathrm{k} \in \mathbb{R}$, $\boldsymbol{\Sigma}_{n\mathrm{k}} \in \mathbb{R}^{B\times B}$ are defined by:

$$\pi_\mathrm{k} := \prod_{j=1}^{M} \pi_{jk_j}, \boldsymbol{\mu}_{n\mathrm{k}} := \sum_{j=1}^{M} \alpha_{nj}\boldsymbol{\mu}_{jk_j}, \boldsymbol{\Sigma}_{n\mathrm{k}} := \sum_{j=1}^{M} \alpha_{nj}^2\boldsymbol{\Sigma}_{jk_j} + \mathrm{D} \tag{3}$$

In the prior of abundances of $p(\mathrm{A})$, GMM assumes the abundances A have the proper smoothness and sparsity prior constraints. The density function of the abundances A can be generalized as follows:

$$p\left(\mathrm{A}\right) \propto \exp\left\{-\tfrac{\beta_1}{2}\mathrm{Tr}\left(\mathrm{A}^T\mathrm{LA}\right) + \tfrac{\beta_2}{2}\mathrm{Tr}\left(\mathrm{A}^T\mathrm{A}\right)\right\}, \tag{4}$$

where L is a *graph Laplacian* matrix constructed from $w_{nm}, n, m = 1, \ldots, N$ with $w_{nm} = e^{||\mathrm{y}_n - \mathrm{y}_m||^2/2\mathrm{B}\eta^2}$ for neighboring pixels and 0 otherwise. Tr is the trace of the matrix, and $\mathrm{Tr}\left(\mathrm{A}^T\mathrm{LA}\right) = \frac{1}{2}\sum_{n,m} w_{nm}||\alpha_n - \alpha_m||^2$, with β_1 controlling smoothness and β_2 controlling sparsity of the abundance maps.

On the basis of the conditional density function and the priors, Bayes' theorem posits the posterior is given by

$$p(\mathrm{A}, \boldsymbol{\Theta}|\mathrm{Y}, \mathrm{D}) \propto p(\mathrm{Y}|\mathrm{A}, \boldsymbol{\Theta}, \mathrm{D})p(\mathrm{A})p(\boldsymbol{\Theta}) \tag{5}$$

where $p(\boldsymbol{\Theta})$ is assumed to be a uniform distribution. Maximizing $p(\mathrm{A}, \boldsymbol{\Theta}|\mathrm{Y}, \mathrm{D})$ equals to minimizing $-\log p(\mathrm{A}, \boldsymbol{\Theta}|\mathrm{Y}, \mathrm{D})$. The GMM method is equivalent to solving the optimization problem as follows:

$$\varepsilon(\mathrm{A}, \boldsymbol{\Theta}) = -\sum_{n=1}^{N} \log \sum_{\mathrm{k}\in\mathcal{K}} \pi_\mathrm{k}\mathcal{N}(\mathrm{y}_n|\boldsymbol{\mu}_{n\mathrm{k}}, \boldsymbol{\Sigma}_{n\mathrm{k}}) + \varepsilon_{\text{prior}}(\mathrm{A}), \tag{6}$$

s.t. $\pi_\mathrm{k} \geqslant 0, \sum_{\mathrm{k}\in\mathcal{K}} \pi_\mathrm{k} = 1, \alpha_{nj} \geqslant 0, \sum_{j=1}^{M} \alpha_{nj} = 1, \forall n$ where $\varepsilon_{\text{prior}} = -\frac{\beta_1}{2}\mathrm{Tr}\left(\mathrm{A}^T\mathrm{LA}\right) + \frac{\beta_2}{2}\mathrm{Tr}\left(\mathrm{A}^T\mathrm{A}\right)$ and $\boldsymbol{\mu}_{n\mathrm{k}}, \boldsymbol{\Sigma}_{n\mathrm{k}}$ are defined in Eq. (3).

2.2. Formulation of the proposed GMM-SS-LRR

The correlations of the adjoining bands and the adjacent pixels are connected in the HSI, and the prior constraints on the abundance A in GMM cannot be used to extract the local spatial information. Thus, we use low-rank property prior constraints on the abundances A after conducting principal component analysis (PCA) and SS of the HSI. Therefore, the priors for abundance A based on the proposed GMM-SS-LRR can be mathematically written as follows:

$$p\left(\mathrm{A}\right) \propto \exp\left\{-\tfrac{\beta_1}{2}\mathrm{Tr}\left(\mathrm{A}^T\mathrm{LA}\right) + \tfrac{\beta_2}{2}\mathrm{Tr}\left(\mathrm{A}^T\mathrm{A}\right) + \tfrac{\beta_3}{2}\mathrm{rank}(\mathrm{A})\right\}. \tag{7}$$

However, Eq. (7) is a non-convex optimization problem, which is difficult to work out or is even NP-hard. We use the nuclear norm to substitute the rank function because this norm is widely used as a surrogate to the rank function. Thus, the prior constraints on A can be reformulated as

$$p\left(\mathrm{A}\right) \propto \exp\left\{-\tfrac{\beta_1}{2}\mathrm{Tr}\left(\mathrm{A}^T\mathrm{LA}\right) + \tfrac{\beta_2}{2}\mathrm{Tr}\left(\mathrm{A}^T\mathrm{A}\right) + \tfrac{\beta_3}{2}||\mathrm{A}||_*\right\}, \tag{8}$$

where $||\mathrm{A}||_*$ denotes the nuclear norm of the matrix A. The proposed GMM-SS-LRR method is equivalent to solving the optimization problem as follows:

$$\begin{aligned}&\varepsilon(\mathrm{A}, \boldsymbol{\Theta}) = -\sum_{n=1}^{N} \log \sum_{\mathrm{k}\in\mathcal{K}} \pi_\mathrm{k}\mathcal{N}(\mathrm{y}_n|\boldsymbol{\mu}_{n\mathrm{k}}, \boldsymbol{\Sigma}_{n\mathrm{k}}) + \varepsilon_{\text{prior}}(\mathrm{A})\\ &\text{s.t. } \pi_\mathrm{k} \geqslant 0, \sum_{\mathrm{k}\in\mathcal{K}} \pi_\mathrm{k} = 1, \alpha_{nj} \geqslant 0, \sum_{j=1}^{M} \alpha_{nj} = 1, \forall n,\end{aligned} \tag{9}$$

where $\varepsilon_{\text{prior}} = -\frac{\beta_1}{2}\mathrm{Tr}\left(\mathrm{A}^T\mathrm{LA}\right) + \frac{\beta_2}{2}\mathrm{Tr}\left(\mathrm{A}^T\mathrm{A}\right) + \frac{\beta_3}{2}||\mathrm{A}||_*$ is defined in Eq. (8) and $\boldsymbol{\mu}_{n\mathrm{k}}, \boldsymbol{\Sigma}_{n\mathrm{k}}$ are defined in Eq. (3).

Following the routine of EM, the E step calculates the posterior probabllity of the latent variable, and the M step maximizes the expected value of the complete data log-likelihood. Accordingly, we can obtain

$$\frac{\partial\varepsilon_M}{\partial\boldsymbol{\mu}_{jl}} = -\sum_{n=1}^{N}\sum_{\mathrm{k}\in\mathcal{K}} \delta_{lk_j}\alpha_{nj}\boldsymbol{\lambda}_{n\mathrm{k}}, \tag{10}$$

$$\frac{\partial\varepsilon_M}{\partial\boldsymbol{\Sigma}_{jl}} = -\sum_{n=1}^{N}\sum_{\mathrm{k}\in\mathcal{K}} \delta_{lk_j}\alpha_{nj}^2\boldsymbol{\Psi}_{n\mathrm{k}}, \tag{11}$$

$$\begin{aligned}\frac{\partial\varepsilon_M}{\partial\alpha_{nj}} =& \sum_{\mathrm{k}\in\mathcal{K}} \boldsymbol{\lambda}_{n\mathrm{k}}^T\boldsymbol{\mu}_{jl_j} - 2\alpha_{nj}\sum_{\mathrm{k}\in\mathcal{K}} \mathrm{Tr}(\boldsymbol{\Psi}_{n\mathrm{k}}^T\boldsymbol{\Sigma}_{jk_j})\\ &+ \beta_1(\mathrm{KA})_{nj} - \beta_3(\mathrm{UV}^T)_{nj},\end{aligned} \tag{12}$$

where $\boldsymbol{\lambda}_{n\mathrm{k}} \in \mathbb{R}^{B\times 1}$ and $\boldsymbol{\Psi}_{n\mathrm{k}} \in \mathbb{R}^{B\times B}$ are given by

$$\boldsymbol{\lambda}_{n\mathrm{k}} = \gamma_{n\mathrm{k}}\boldsymbol{\Sigma}_{n\mathrm{k}}^{-1}(\mathrm{y}_n) - \boldsymbol{\mu}_{n\mathrm{k}}, \tag{13}$$

$$\boldsymbol{\Psi}_{n\mathrm{k}} = \tfrac{1}{2}\gamma_{n\mathrm{k}}\boldsymbol{\Sigma}_{n\mathrm{k}}^{-T}(\mathrm{y}_n - \boldsymbol{\mu}_{n\mathrm{k}})(\mathrm{y}_n - \boldsymbol{\mu}_{n\mathrm{k}}^T)\boldsymbol{\Sigma}_{n\mathrm{k}}^{-T} - \tfrac{1}{2}\gamma_{n\mathrm{k}}\boldsymbol{\Sigma}_{n\mathrm{k}}^{-T}, \tag{14}$$

and the $\mathrm{K} = \mathrm{L} - \frac{\beta_2}{\beta_1}\mathrm{I}_N$ (suppose $\beta_1 \neq 0$), U,V is the singular value decomposition of the abundance A. Considering that we have the non-negatively and sum-to-one constraint to α_{nj} and positive definite constraint of $\mathbf{\Sigma}_{jk}$, minimizing $\varepsilon(\mathrm{A}, \mathbf{\Theta})$ becomes very difficult. Therefore, in each M step, we only decrease this objective function by *project gradient decent* [14]. Given the complexity of EM scheme in solving GMM-SS-LRR, the most time-consuming step is estimating the abundances A in each iteration. Thus, the EM complexity of GMM-SS-LRR has spatial complexity $\mathcal{O}(NB^2)$ and time complexity $\mathcal{O}(NB^3)$.

3. EXPERIMENTAL RESULT

In this section, we implemented the algorithm in MATLAB and compared the proposed GMM-SS-LRR with GMM, NCM and BCM on synthetic datasets and real HSI. For our method and GMM, the original image data were projected to subspace with 10 dimensions to speed up the computation for abundance estimation. All the compared method code were downloaded from the website and the code parameters were set same as the original code.

For the synthetic data experiments, we use the spectral library randomly selected from the ASTER spectral library [15], which determined a spectral range from $0.4\mu m$ to $14\mu m$, the size of the synthetic is 60×60 pixels and constructed from 5 endmembers: limestone, basalt, concrete, conifer, asphalt whose spectral signatures were highly differentiable. We made the first material as background, The procedure of generating the abundances maps followed [16]: for each other material 400 Gaussian blobs were both randomly placed at the corner. The parameter of the proposed method GMM-SS-LRR for the synthetic data is $\beta_1 = 0.1, \beta_2 = 0.1, \beta_3 = 0.01$.

For the real data experiments, we have selected two HSI datasets to compare. In order to compare with other methods, in the first real HSI, We choose the same dataset and ROI as selected in the GMM method[11]: the data was collected over Mississippis-Gulfpark Campus. It is a 271 by 284 image with 72 bands corresponding to wavelengths 0.368μm to 1.043μm. The spatial resolution is 1 meter/pixel. And ROI is 58×65 which contains 5 material: road, shadow, building, grass, and tree. And the second real HSIs was collected over the Urban dataset [17], which is 307×307 pixels with 210 wavelengths ranging from 400 nm to 2500 nm. The spatial resolution is 2×2 m^2 area. All the parameters of the proposed method GMM-SS-LRR for the real data were set to $\beta_1 = 5, \beta_2 = 5, \beta_3 = 1$, The errors of abundances for these algorithms are shown in Table I, Table II, and Table III, which implies that GMM-SS-LRR performed best overall both in synthetic and real datasets.

Fig. 1 shows the abundance maps comparison in the Gulfport dataset. Comparing them with the ground truth (the first group of Fig. 1). We can see that BCM failed to estimate the pure pixels of the Tree, although ground truth pure pixels were used for training. For example, the second and third abundances maps of BCM show that the pixels of Trees are mixed with Asphalt. For the BCM and NCM, we haven't use PCA to get the main information to for the dataset while use the original HSI dataset as input. However, they still performance poor in this dataset. The result of GMM-SS-LRR not only shows sparse abundances for the region but also interprets the boundary as a combination of neighboring material. Although the results of GMM method look good in general, the abundances in a pure material region are inconsistent. The errors of abundances for these algorithms are shown in Table II, which implies that GMM-SS-LRR performed best overall.

Fig. 2 shows the abundance maps in the Urban dataset compared with other algorithms. We can see that our proposed method GMM-SS-LRR matches the groud truth (the first group of Fig. 2) best, followed by GMM. This is also verified in the quantitative analysis in Table III. And the incomplete region of Road for the NCM (Tree for the BCM) show their insufficiency in this case.

Table 1: Abundance errors for synthetic dataset

$\times10^{-4}$	GMM-SS-LRR	GMM	NCM	BCM
Limestone	**65**	177	470	640
Basalt	**25**	33	205	230
Concrete	**37**	103	331	443
Conifer	**19**	25	178	204
Asphalt	**21**	32	189	194
Mean	**33**	74	229	342

Table 2: Abundance errors for Gulfport dataset

$\times10^{-4}$	GMM-SS-LRR	GMM	NCM	BCM
Limestone	**401**	1089	1270	1374
Basalt	**378**	512	1789	1574
Concrete	767	**652**	2479	2521
Conifer	665	**582**	1649	1515
Asphalt	**118**	170	792	606
Mean	**465**	601	1552	1518

Table 3: Abundance errors for Urban dataset

$\times10^{-4}$	GMM-SS-LRR	GMM	NCM	BCM
Limestone	**827**	1378	1896	2602
Basalt	**489**	654	792	1427
Concrete	**240**	453	407	551
Conifer	**608**	729	2017	3117
Asphalt	**713**	902	3342	3558
Mean	**575**	823	1690	2251

4. CONCLUSIONS

In this paper, we proposed a GMM-SS-LRR method for linear unmixing of HSI, which can take the underlying low-

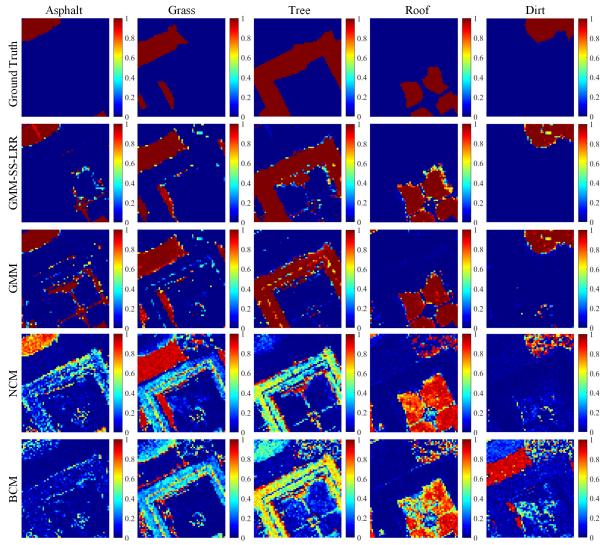

Fig. 1: Abundance maps for the Gulfport dataset. From top to bottom: Groud Truth, GMM-SS-LRR, GMM, NCM, BCM. The corresponidng endmembers from left to right are Asphalt, Grass, Tree, Roof and Dirt.

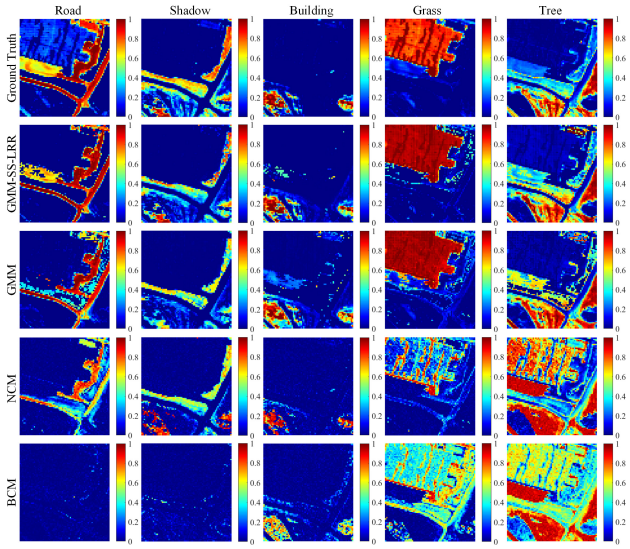

Fig. 2: Abundance maps for the Urban dataset. From top to bottom: Groud Truth, GMM-SS-LRR, GMM, NCM, BCM. The corresponidng endmembers from left to right are Road, Shadow, Building, Grass and Tree.

rank property of abundances in each homogeneous region into account, and adapt the adaptive size superpixel strategy to make the unmixing region's shape and size be accustomed on the basis of different spatial structures. Moreover, with low-rank constraints on the abundances, the conditional density function leads to a MAP problem which can be solved using GEM method. And the experiments on both synthetic datasets and real HSI demonstrate that proposed GMM-SS-LRR is efficient for solving the hyperspectral unmixing problem compared with the other algorithms.

5. REFERENCES

[1] Jiayi Ma, Huabing Zhou, Ji Zhao, Yuan Gao, Junjun Jiang, and Jinwen Tian, "Robust feature matching for remote sensing image registration via locally linear transforming," *IEEE TGRS*, vol. 53, no. 12, pp. 6469–6481, 2015.

[2] Xiaoguang Mei, Yong Ma, Fan Fan, Chang Li, Chengyin Liu, Jun Huang, and Jiayi Ma, "Infrared ultraspectral signature classification based on a restricted boltzmann machine with sparse and prior constraints," *IJRS*, vol. 36, no. 18, pp. 4724–4747, 2015.

[3] Fan Fan, Yong Ma, Chang Li, Xiaoguang Mei, Jun Huang, and Jiayi Ma, "Hyperspectral image denoising with superpixel segmentation and low-rank representation," *Inf. Sci.*, vol. 397, pp. 48–68, 2017.

[4] Jiayi Ma, Junjun Jiang, Huabing Zhou, Ji Zhao, and Xiaojie Guo, "Guided locality preserving feature matching for remote sensing image registration," *IEEE TGRS*, vol. 56, no. 8, pp. 4435–4447, 2018.

[5] Xiaoguang Mei, Yong Ma, Chang Li, Fan Fan, Jun Huang, and Jiayi Ma, "Robust gbm hyperspectral image unmixing with superpixel segmentation based low rank and sparse representation," *Neurocomputing*, vol. 275, pp. 2783–2797, 2018.

[6] O. Eches, N. Dobigeon, C. Mailhes, and J.-Y. Tourneret, "Bayesian estimation of linear mixtures using the normal compositional model. application to hyperspectral imagery," *IEEE TIP*, vol. 19, no. 6, pp. 1403–1413, June 2010.

[7] David Stein, "Application of the normal compositional model to the analysis of hyperspectral imagery," in *Advances in Techniques for Analysis of Remotely Sensed Data*, 2003, pp. 44–51.

[8] Abderrahim Halimi, Nicolas Dobigeon, and Jean-Yves Tourneret, "Unsupervised unmixing of hyperspectral images accounting for endmember variability," *IEEE TIP*, vol. 24, no. 12, pp. 4904–4917, 2015.

[9] Bing Zhang, Lina Zhuang, Lianru Gao, Wenfei Luo, Qiong Ran, and Qian Du, "Pso-em: A hyperspectral unmixing algorithm based on normal compositional model," *IEEE TGRS*, vol. 52, no. 12, pp. 7782–7792, 2014.

[10] Xiaoxiao Du, Alina Zare, Paul Gader, and Dmitri Dranishnikov, "Spatial and spectral unmixing using the beta compositional model," *IEEE JSTARS*, vol. 7, no. 6, pp. 1994–2003, 2014.

[11] Yuan Zhou, Anand Rangarajan, and Paul D Gader, "A gaussian mixture model representation of endmember variability in hyperspectral unmixing," *IEEE TIP*, vol. 27, no. 5, pp. 2242–2256, 2018.

[12] Qing Qu, Nasser M Nasrabadi, and Trac D Tran, "Abundance estimation for bilinear mixture models via joint sparse and low-rank representation," *IEEE TGRS*, vol. 52, no. 7, pp. 4404–4423, 2014.

[13] Xiao-Li Meng and Donald B Rubin, "Maximum likelihood estimation via the ecm algorithm: A general framework," *Biometrika*, vol. 80, no. 2, pp. 267–278, 1993.

[14] Gregory P Asner and Kathleen B Heidebrecht, "Spectral unmixing of vegetation, soil and dry carbon cover in arid regions: comparing multispectral and hyperspectral observations," *IJRS*, vol. 23, no. 19, pp. 3939–3958, 2002.

[15] AM Baldridge, SJ Hook, CI Grove, and G Rivera, "The aster spectral library version 2.0," *RSE*, vol. 113, no. 4, pp. 711–715, 2009.

[16] Yuan Zhou, Anand Rangarajan, and Paul D Gader, "A spatial compositional model for linear unmixing and endmember uncertainty estimation," *IEEE TIP*, vol. 25, no. 12, pp. 5987–6002, 2016.

[17] Feiyun Zhu, Ying Wang, Bin Fan, Gaofeng Meng, and Chunhong Pan, "Effective spectral unmixing via robust representation and learning-based sparsity," *CoRR*, vol. abs/1409.0685, 2014.